Spectrochimica Acta Part A: Molecular and Biomolecular Spectroscopy 302 (2023) 123121



Contents lists available at ScienceDirect

Spectrochimica Acta Part A:
Molecular and Biomolecular Spectroscopy

journal homepage: www.journals.elsevier.com/spectrochimica-acta-part-a-molecular-and-biomolecular-spectroscopy





CRISPR/Cas12a and G-quadruplex DNAzyme-driven multimodal biosensor for visual detection of Aflatoxin B1

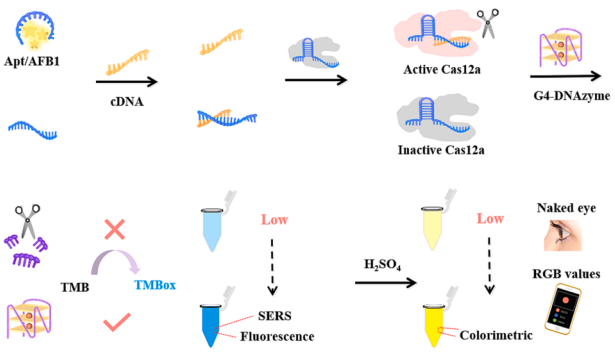
Zhihui Wu [a,b,c], Da-Wen Sun [a,b,c,d,*], Hongbin Pu [a,b,c]

[a] School of Food Science and Engineering, South China University of Technology, Guangzhou 510641, China
[b] Academy of Contemporary Food Engineering, South China University of Technology, Guangzhou Higher Education Mega Center, Guangzhou 510006, China
[c] Engineering and Technological Research Centre of Guangdong Province on Intelligent Sensing and Process Control of Cold Chain Foods, & Guangdong Province Engineering Laboratory for Intelligent Cold Chain Logistics Equipment for Agricultural Products, Guangzhou Higher Education Mega Centre, Guangzhou 510006, China
[d] Food Refrigeration and Computerized Food Technology (FRCFT), Agriculture and Food Science Centre, University College Dublin, National University of Ireland, Belfield, Dublin 4, Ireland

HIGHLIGHTS

- A highly sensitive, specific, and low-cost detection strategy was developed.
- G4-DNAzyme added Cas12a system achieved a simultaneous output of three signals.
- G4-DNAzyme-based sensor realized smartphone-assisted portable detection of AFB1.
- The sensor correctly identified negatives and positives from peanut samples.

GRAPHICAL ABSTRACT



ARTICLE INFO

Keywords:
Aflatoxin B1
CRISPR/Cas12a
G4-DNAzyme
Multimodal
Biosensor

ABSTRACT

Aflatoxin B1 (AFB1) contamination severely threatens human and animal health, it is thus critical to construct a strategy for its rapid, accurate, and visual detection. Herein, a multimodal biosensor was proposed based on CRISPR/Cas12a cleaved G-quadruplex (G4) for AFB1 detection. Briefly, specific binding of AFB1 to the aptamer occupied the binding site of the complementary DNA (cDNA), and cDNA then activated Cas12a to cleave G4 into fragments. Meanwhile, the intact G4-DNAzyme could catalyze 3, 3′, 5, 5′-tetramethylbenzidine (TMB) to form colourimetric/SERS/fluorescent signal-enhanced TMBox, and the yellow solution produced by TMBox under acidic conditions could be integrated with a smartphone application for visual detection. The colourimetric/SERS/fluorescent biosensor yielded detection limits of 0.85, 0.79, and 1.65 pg·mL^{-1}, respectively, and was applied for detecting AFB1 in peanut, maize, and badam samples. The method is suitable for visual detection in naturally contaminated peanut samples and has prospective applications in the food industry.

* Corresponding author.
E-mail address: dawen.sun@ucd.ie (D.-W. Sun).
URL: http://www.ucd.ie/refrig, http://www.ucd.ie/sun (D.-W. Sun).

https://doi.org/10.1016/j.saa.2023.123121
Received 2 May 2023; Received in revised form 6 July 2023; Accepted 7 July 2023
Available online 8 July 2023
1386-1425/© 2023 The Author(s). Published by Elsevier B.V. This is an open access article under the CC BY license (http://creativecommons.org/licenses/by/4.0/).

1. Introduction

Aflatoxin B1 (AFB1), a group I carcinogen primarily generated by *Aspergillus flavus* and *Aspergillus parasiticus* [1,2], is considered the major mycotoxin commonly found in agricultural and food products. AFB1 is difficult to degrade due to its high thermal stability [3]. In addition, carcinogenic, mutagenic, and teratogenic diseases caused by the ingestion of AFB1-contaminated foods have become a global public health concern [4], therefore, rapid and accurate detection of AFB1 is very significant. At present, conventional analytical approaches mainly include chromatography, chromatography/mass spectrometry, immunoassay, etc. [5,6]. Although these techniques exhibit superiority in terms of high accuracy and reproducibility, they have some defects such as tedious operation, low sensitivity, labour intensiveness, and unsuitability for field detection [7]. Therefore, the demand for efficient, rapid, and field-deployable detection of AFB1 is increasing.

In recent years, clustered regularly interspaced short palindromic repeats (CRISPR) and CRISPR-associated nuclease (Cas) systems are significant adaptive immune systems for bacteria and archaea [8], and have been increasingly utilized for gene editing [9], medical diagnostics [10] and biosensors [11]. A typical example is the DETECTR (DNA endonuclease-targeted CRISPR trans reporter) technique [12] based on the unique *trans*-cleavage single-stranded DNA (ssDNA) activity of Cas12a protein. Remarkably, the guide RNA (crRNA) of Cas12a (Cpf1) can precisely recognize double-stranded DNA (dsDNA) or ssDNA by base complementary pairing, and then activate Cas12a to *trans*-cleavage ssDNA reporter, thus achieving conversion of target DNA information into readable ssDNA reporter signals [12,13]. Currently, most of the constructed CRISPR/Cas12a biosensing platforms have the merits of simple preparation, specificity, and high detection efficiency, and have been widely applied for nucleic acid detection [14–16], while small molecule detection is still at the early stage.

Fortunately, some small molecules always have specific single-stranded aptamers, thus providing an opportunity to transduce small molecules into ssDNA information [11]. For instance, Wang et al. [17] immobilised OTA aptamer on Fe_3O_4@Au magnetic beads to convert small molecule signals into aptamer information, resulting in the output of electrochemiluminescent and fluorescent signals. Meanwhile, Wang et al. [18] also hybridised the AFB1 aptamer with cDNA into dsDNA, and upon the addition of AFB1, the aptamer tended to form the aptamer-AFB1 complex, resulting in a change in the output signal. In this study, the detection limit of this strategy was as low as 5 $pg{\cdot}mL^{-1}$ in the photothermal mode. In addition, Qiao et al. [19] proposed an "aptamer-locker" CRISPR/Cas12a biosensor for the sensitive determination of melamine with a limit of detection (LOD) of 38 nM. Moreover, the entire detection process took only 20 min and did not require complex sample pre-treatment. Recently, Lin et al. [20] constructed a Cas12a-based luminescence resonance energy transfer biosensor for the quantification of deoxynivalenol (DON) in corn flour and Tai Lake water samples with a LOD of 0.64 $ng{\cdot}mL^{-1}$ and showed that DON aptamer triggered the cleavage of ssDNA on upconversion nanoparticles by Cas12a, which caused changes in the upconversion luminescence (UCL) signal, and the method has a sensitive and specific detection workflow. Numerous studies [21–23] have demonstrated that the CRISPR/cas12a biosensors exhibit distinct advantages toward small molecule analysis. Nevertheless, these strategies typically utilize fluorophore- and quencher-labelled ssDNA (FQ-ssDNA) as reporters, which dramatically increased the cost of detection.

G-quadruplex (G4) is a four-stranded nucleic acid structure consisting of G-rich sequences in the presence of K^+ or Na^+, and the DNAzyme with peroxidase-like activity formed by the binding of G4 to hemin can catalyze 3, 3′, 5, 5′-tetramethylbenzidine (TMB) to form a blue solution of TMB_{OX} [24]. However, the catalytic ability of G4-DNAzyme may be deprived after the G4 is cleaved. To date, several G4-DNAzyme-based sensing platforms have been proposed for visual detection [25–27], and the signal outputs of these studies were limited to a single colourimetric signal, which was susceptible to interference from experimental instruments and human manipulation. Therefore, the construction of CRISPR biosensors with multiple signal outputs is essential to obtain reliable and robust performance [28].

CRISPR/Cas12a-based biosensors have realized diverse signal transduction modalities, including colourimetry [26], Raman spectroscopy [29–32], fluorescence spectroscopy [11,33], electrochemistry [13], lateral flow strips [34], and so forth, and TMB_{OX} is not only a blue solution visible to the naked eye but also features SERS and fluorescence effects [35]. For example, Qian et al. [36] achieved a colourimetric detection of AFB1 in corn samples with a LOD of 35 $pg{\cdot}mL^{-1}$, based on the principle that AuNPs can catalyse the oxidation of TMB by H_2O_2 to generate a coloured product. Therefore, the G4-DNAzyme integrated CRISPR/Cas12a system can cleverly realize colourimetric, SERS, and fluorescent triple-channel sensing. To enhance the portability of the biosensor, the colourimetric signal could be integrated into the colour-assist application (App) in a smartphone, which may provide a prospective approach for the point-of-care test (POCT). Besides, silver nanoparticles (AgNPs) with strong SERS activity are usually preferred as enhanced substrates [7,37–39]. In summary, G4-DNAzyme-based biosensors should offer remarkable benefits, especially in terms of reliable detection, multi-signal sensing, and field deployability.

Therefore, in the current study, a smartphone-assisted multimodal sensor was designed based on Cas12a combined with G4-DNAzyme for the detection of AFB1. Firstly, the preferential binding of AFB1 to the aptamer changed the conformation of the aptamer and the complementary DNA (cDNA) was in an unbound state, and the higher the concentration of AFB1, the higher the concentration of free cDNA. Secondly, the cDNA was designed to complementarily pair with Cas12a/crRNA bases to form a ternary complex for activating the *trans*-cleavage activity of Cas12a. Thirdly, the G4 served as the cleavage substrate of Cas12a/crRNA. In general, the intact G4/hemin composite exhibited a peroxidase-like activity that catalyzes the formation of blue TMBox from colourless TMB and then terminated the catalytic reaction under acidic conditions to produce the yellow TMBox. Thus, as the concentration of AFB1 increased, more cDNA activated the cleavage of G4 by Cas12a. As the result, the disrupted G4 was deprived of peroxidase-like activity, leading to a gradual weakening of the colourimetric intensity of yellow TMBox, the SERS intensity under AgNPs substrate, and the fluorescent intensity of blue TMBox. Collectively, this sensing platform did not require a chemically labelled reporter, thereby reducing the complexity and economic cost of the assay, the precise identification of cDNA and crRNA ensured the accuracy of AFB1 assay, the superior cleavage capability of Cas12a improved the sensitivity of the assay, and the smartphone-assisted colourimetric readout enabled portable detection.

2. Materials and methods

2.1. Chemicals and reagents

Lachnospiraceae bacterium Cas12a (LbCas12a, cpf1) was supplied from Tolo Biotechnology Co., Ltd. (Shanghai, China). All the nucleic acid sequences, DNA marker (25–50 bp), 4S gel red nucleic acid dye, hemin, and DEPC-treated nuclease-free water were supplied by Sangon Biotech Co., Ltd. (Shanghai, China). KCl, NaCl, $MgCl_2$, $NH_2OH{\cdot}HCl$, and TMB were purchased from Shanghai Macklin Biochemical Co., Ltd. (Shanghai, China). H_2O_2, H_2SO_4, NaOH, and $AgNO_3$ were obtained by Sinopharm Chemical Reagent Co., Ltd. (Shanghai, China). 15% native polyacrylamide gel electrophoresis (PAGE) precast gel, 1 × TBE running buffer, and 5 × TBE loading buffer were acquired from Shanghai Wansheng Haotian Biotechnology Co., Ltd. (Shanghai, China). 1 M RNase-free Tris-HCl (pH 7.6) and 1 × HEPES buffer (25 mM HEPES, 20 mM KCl, 200 mM NaCl, and 0.05% Triton X-100, pH 5.3) were obtained from Beijing Noble Ryder Technology Co., Ltd. (Beijing, China). A commercial enzyme-linked immunosorbent assay (ELISA) kit and colloidal gold-based rapid test card for AFB1 were bought from Shenzhen Finder

Biotech Co., Ltd. (Shenzhen, China). All relevant mycotoxins were purchased from TanMo Quality Testing Technology Co., Ltd. (Beijing, China). Fresh peanuts, maize, and badam were bought from a local supermarket (Guangzhou, China). DEPC-treated nuclease-free water was used for the whole experiment, and all reactions were performed in RNase-free tubes. Deionized water purified by a Milli-Q system (Millipore Co., Billerica, MA, USA) was used for the preparation of AgNPs.

Buffer solutions prepared during the experiment included buffer $Mg^{2+} + K^+$ consisting of 10 mM Tris-HCl, 70 mM KCl and 10 mM $MgCl_2$, buffer K^+ consisting of 10 mM Tris-HCl and 70 mM KCl, buffer Mg^{2+} consisting of 50 mM Tris-HCl and 10 mM $MgCl_2$, and buffer $Mg^{2+} + Na^+$ consisting of 50 mM Tris-HCl, 150 mM NaCl and 2 mM $MgCl_2$. All the buffers had a pH of 7.6.

Sequences of DNA or RNA strands sequence used for the established biosensor were as follows:

Aptamer-AFB1: 5′-GTTGGGCACGTGTTGTCTCTCTGTGTCTCGTGCCCTTCGCTAGGCCC-3′;
cDNA: 5′-CAGAGAGACAACACGTGCCCAAC-3′;
cDNA-2: 5′-CAGAGACTCAACACGTGCCCAAC-3′;
cDNA-4: 5′-CAGAGACTGTACACGTGCCCAAC-3′;
cDNA-6: 5′-CAGAGACTGTTGACGTGCCCAAC-3′;
cDNA-8: 5′-CAGAGACTGTTGTGGTGCCCAAC-3′;
G4-ssDNA: 5′-TTAGGGTTAGGGTTAGGGTTAGGGTTA-3′;
FQ-ssDNA: 5′-FAM-TTATT-HBQ1-3′;
crRNA: 5′-UAAUUUCUACUAAGUGUAGAUGUUGGGCACGUGUUGUCUCU-3′.

2.2. Instruments

Ultraviolet–visible (UV–vis) absorbance spectra were recorded by a UV–vis spectrometer (UV-1800, Shimadzu Co., Kyoto, Japan). All the SERS spectra were acquired with a laser confocal microscope Raman system (LabRAM HR, Horiba France SAS, Villeneuve d'Ascq, France) equipped with a He-Ne laser wavelength of 633 nm and a 10 × objective lens. Raman spectra were acquired in the range of 1100∼1800 cm^{-1} with an integration time of 2 s. All fluorescence spectra were acquired using an RF-6000 fluorescence spectrophotometer (Shimadzu Co., Kyoto, Japan). TEM image of AgNPs was obtained by a high-resolution transmission electron microscope (JEM-2100F, JEOL Ltd., Tokyo, Japan). The circular dichroism (CD) spectra of AFB1, aptamer, aptamer/AFB1, G4, and G4 fragments were acquired with a CD spectrometer (JASCO Co., Tokyo, Japan) at the spectral region from 200 to 350 nm.

2.3. Preparation of AgNPs

AgNPs were synthesized as per the method reported in the literature [37]. Briefly, 5 mL of 0.30 M $NH_2OH{\cdot}HCl$ was dissolved in a conical flask containing 84 mL deionized water, and 1 mL of 0.60 M NaOH was introduced under the magnetic stirring by a magnetic heating stirrer (DF-101S, Gongyi Yuhua Instrument Co., Ltd., Zhengzhou, China). After that, 10 mL of 0.01 M $AgNO_3$ solution was quickly added under vigorous stirring. The reaction mixture was stirred continuously for another 1 h. The final prepared AgNPs were stored away from light in a refrigerator (BCD-539 wt, Haier Group, Shandong, China) at 4 °C for subsequent use.

2.4. FQ reporter-based fluorescent biosensor

To verify the *trans*-cleavage performance of Cas12a, the fluorescence assay was first performed using the FQ-ssDNA reporter as the cleavage substrate [40]. For AFB1 detection, a competitive reaction between cDNA and AFB1 with aptamer was carried out, 10 μL of different concentrations of AFB1 was incubated with 10 μL of 130 nM aptamer at 25 °C for 30 min, and then 10 μL of 150 nM cDNA was added and incubated at 25 °C for another 10 min to form 30 μL of AFB1 competition solution. Meanwhile, 600 nM Cas12a was incubated with 900 nM crRNA in 10 μL buffer ($Mg^{2+} + K^+$) solution at 37 °C for 10 min to assemble the inactivated Cas12a/crRNA complex, and then 1 μL of 12 μM FQ-ssDNA reporter and 59 μL buffer ($Mg^{2+} + K^+$) solution was added and incubated for 35 min at 37 °C. After that, the above-mixed solution was heated at 60 °C for 10 min to stop the enzymatic reaction and recorded by the fluorescence spectrometer (λex: 494 nm, λem: 520 nm).

2.5. G4-DNAzyme reporter-based multimodal biosensor

The G4-DNAzyme-based CRISPR/Cas12a cleavage system was first prepared [41], 1 μM of G4-ssDNA was dissolved in 10 μL of buffer ($Mg^{2+} + K^+$) solution and heated to 95 °C for 5 min using a polymerase chain reaction (PCR) thermocycler (TC1000-G/TC1000-S, Beijing Labgic Technology Co., Ltd. Beijing, China) and cooled to 25 °C to form the secondary structure of G4. Then, 30 μL AFB1 competitive solution and 10 μL of inactivated Cas12a/crRNA complex were performed as previously mentioned. Finally, 50 μL of the mixed cleavage solution was incubated for 35 min at 37 °C in a PCR thermocycler and then heated to 60 °C for 10 min to terminate the cleavage of G4.

For preparing the multimodal signal output system [25,26], 5 μL of 50 μM hemin and 37 μL 1 × HEPES buffer were added to the 50 μL of cleavage system and incubated for 30 min at 37 °C in the dark, then 4 μL of 20 mM TMB and 4 μL of 100 mM H_2O_2 were introduced sequentially. The generated blue TMBox solution was measured directly using a fluorescence spectrometer (λex: 274 nm, λem: 405 nm) after 10 min, and the mixture of 10 μL blue TMBox solution and the synthesized 10 μL AgNPs substrate was detected by Raman spectroscopy. Finally, the colour development reaction was terminated by adding 100 μL of 1 M H_2SO_4 to 100 μL of blue TMBox solution, and the colour of the 200 μL yellow TMBox solution was visualized by the naked eye. Also, the obtained yellow TMBox solution was measured by UV–vis spectroscopy. The RGB (red, green, and blue) values of the yellow TMBox solution were analyzed by a colour-assist App on a smartphone (FTL apps, Inc.) [42]. The different concentrations of AFB1 were quantified according to the change in the B value in the RGB readout.

2.6. Specificity evaluation

The specificity of the constructed method was evaluated by testing buffer ($Mg^{2+} + K^+$) solution (blank sample), 1 ng·mL^{-1} of AFB1, and 10 ng·mL^{-1} of three similar toxins (AFB2, AFG1, and AFG2) under the same experimental parameters. To test the anti-interfering ability of the established FQ-ssDNA-based and G4-DNAzyme-based biosensors, 10 μL of a mixed solution containing 1 ng·mL^{-1} of AFB1 and 10 ng·mL^{-1} of three similar toxins (AFB2, AFG1, and AFG2).

2.7. Spiked and real sample evaluation

In the spiked sample assay, peanut, maize, and badam samples were pretreated as previously described [5]. Briefly, 5 g of food samples were mashed and 10 mL of 70% aqueous methanol solution was added. The above sample solution was sonicated for 10 min and then centrifuged by a high-speed refrigerated centrifuge (JW-3024HR, Anhui Jiaven Equipment Industry Co., Ltd., Hefei, China) at 12000 rpm for 20 min to obtain 1 mL of supernatant. The high concentration of AFB1 standard solution was diluted with the obtained 1 mL of supernatant to form spiked samples with final concentrations of 10, 1, and 0.1 ng·mL^{-1}, respectively. In general, the recovery ratio experiments were conducted similarly by replacing AFB1 standard samples with AFB1 spiked samples, while the accuracy of the sensor was verified with an ELISA kit.

To confirm the practical application capability of the sensor in real samples [3], seven peanut samples without *Aspergillus* or with different amounts of *Aspergillus* were chosen. Simply, the crushed 2 g of peanut samples were added to 5 mL of 70% methanol aqueous solution and shaken for 5 min, then centrifuged at 4000 rpm for 15 min, and 0.5 mL of supernatant was diluted twice with deionized water. Based on European

Union (EU) standards (12 ppb), AFB1 concentrations above 12 ng·mL^{-1} are considered positive. Therefore, the acquired 7 real samples were first screened for positive and negative with a colloidal gold rapid test card, and then the application performance was verified with the multimodal biosensor.

2.8. Gel electrophoresis experiment and imaging

Electrophoresis experiments were carried out using 15% native PAGE [43]. Prepared samples were mixed with 1 × loading buffer and loaded into different lanes of the PAGE precast gel in the electrophoresis instrument (XCell *SureLock* Mini-cell, Thermo Fisher Scientific Ltd., Shanghai, China). The electrophoresis procedure was run with 1 × TBE buffer as the running buffer for 55 min at 120 V. The precast gels were then removed and stained in the nucleic acid dye for 1 h, followed by imaging with a gel imaging system (Fusion Solo S, Vilber Lourmat Sté, Collégien, France).

2.9. Data processing

All experiments were conducted in three replicates and results were expressed as mean ± standard deviation. Relative UV–vis absorbance signal was given as ΔAbs (ΔAbs = Abs_0 − Abs), where Abs Abs_0 represent the UV–vis absorbance intensity of the blue TMBox solution at a wavelength of 405 nm in the presence and absence of AFB1, respectively. ΔI and ΔF represent the SERS relative intensity and fluorescence relative intensity. The schematic diagram was performed using 3ds Max 2020 (Aotodesk Inc., San Rafael, CA, USA). All graphs were acquired using OriginPro 2018 (OriginLab Co., Northampton, MA, USA).

LOD was calculated according to the following equation [5]:

$$LOD = 3S_b + Y_b \quad (1)$$

where S_b is the standard deviation of ΔAbs/ΔI/ΔF of blank samples, and Y_b is the mean of ΔAbs/ΔI/ΔF of the blank samples.

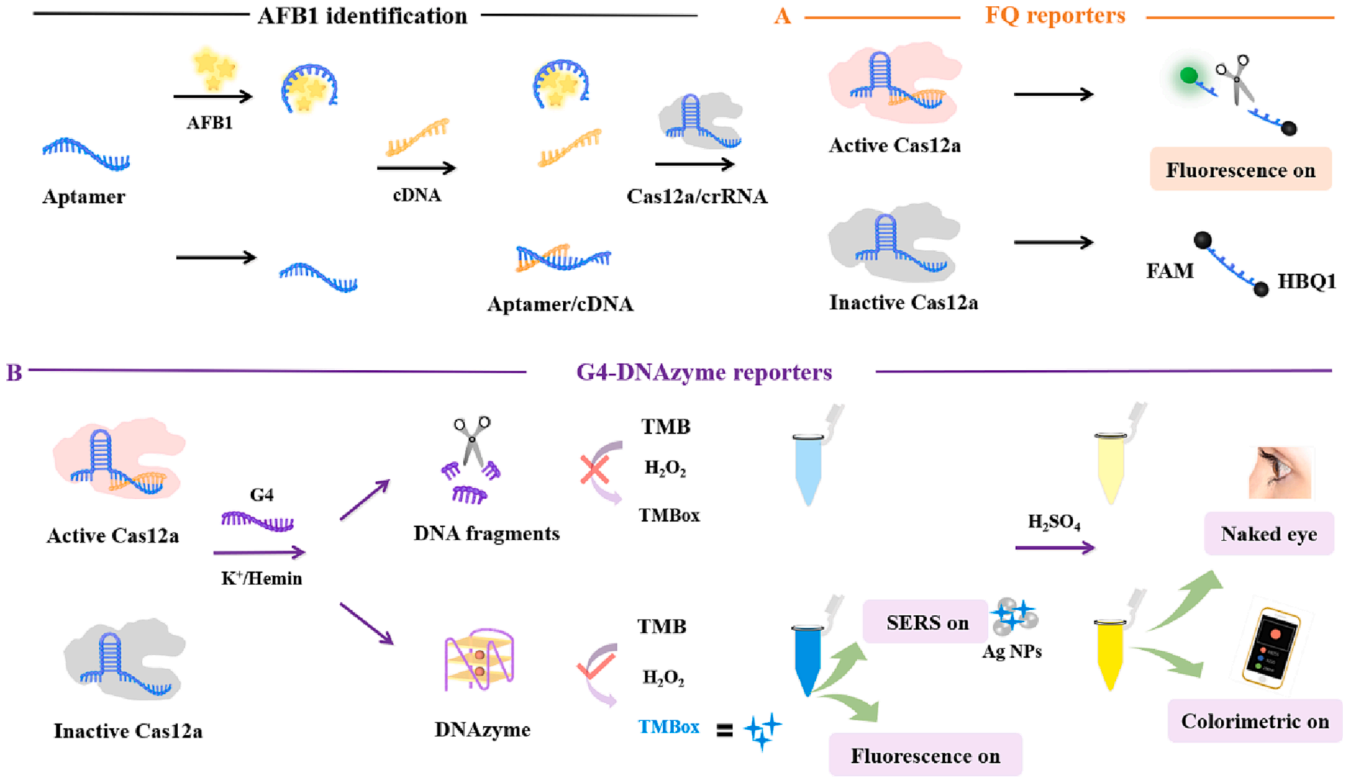
3. Results and discussion

3.1. Detection principle

The multimodal sensor based on CRISPR/Cas12a coupled with G4-DNAzyme for detecting AFB1 is demonstrated in Scheme 1. The biosensor involved three processes: target identification, *trans*-cleavage of G4, and signal output. Firstly, the cDNA strand was designed to be base complementary to both the aptamer and the crRNA. When AFB1 was introduced into the system, the high-affinity binding of AFB1 to the aptamer occupied the binding site of the cDNA, failing to bind the cDNA to the conformationally altered aptamer. Consequently, the free cDNA could precisely recognize crRNA, which then activated the activity of Cas12a *trans*-cleaved G4. The fragmented G4 strand failed to form a DNAzyme with peroxidase-like properties with hemin, which further inhibited the reaction that catalyzes TMB to generate TMB_{OX} solution with SERS and fluorescence effects. On the contrary, the intact G4 could bind hemin to form a G4-DNAzyme in the absence of cDNA. Based on this, the colourimetric/SERS/fluorescent signal was negatively correlated with the concentration of cDNA. What's more, the colourimetric signal could not only be observed by the naked eye but also integrated with the colour-assist app in a smartphone for portable detection.

3.2. Characterization of AgNPs substrate

To investigate the microstructure of the AgNPs substrate, characterization was performed using TEM and UV–vis spectroscopy. The TEM image of Fig. 1A shows the monodisperse morphology of 30 nm AgNPs, demonstrating the successful synthesis of AgNPs substrate. As displayed in Fig. 1B, the UV–vis spectra of AgNPs showed a significant absorption at 402 nm, which was attributed to the surface plasmon absorption peak of AgNPs [37].



Scheme 1. Schematic illustration of CRISPR/Cas12a biosensor based on conventional FQ reporter and G4-DNAzyme reporter for the detection of AFB1.

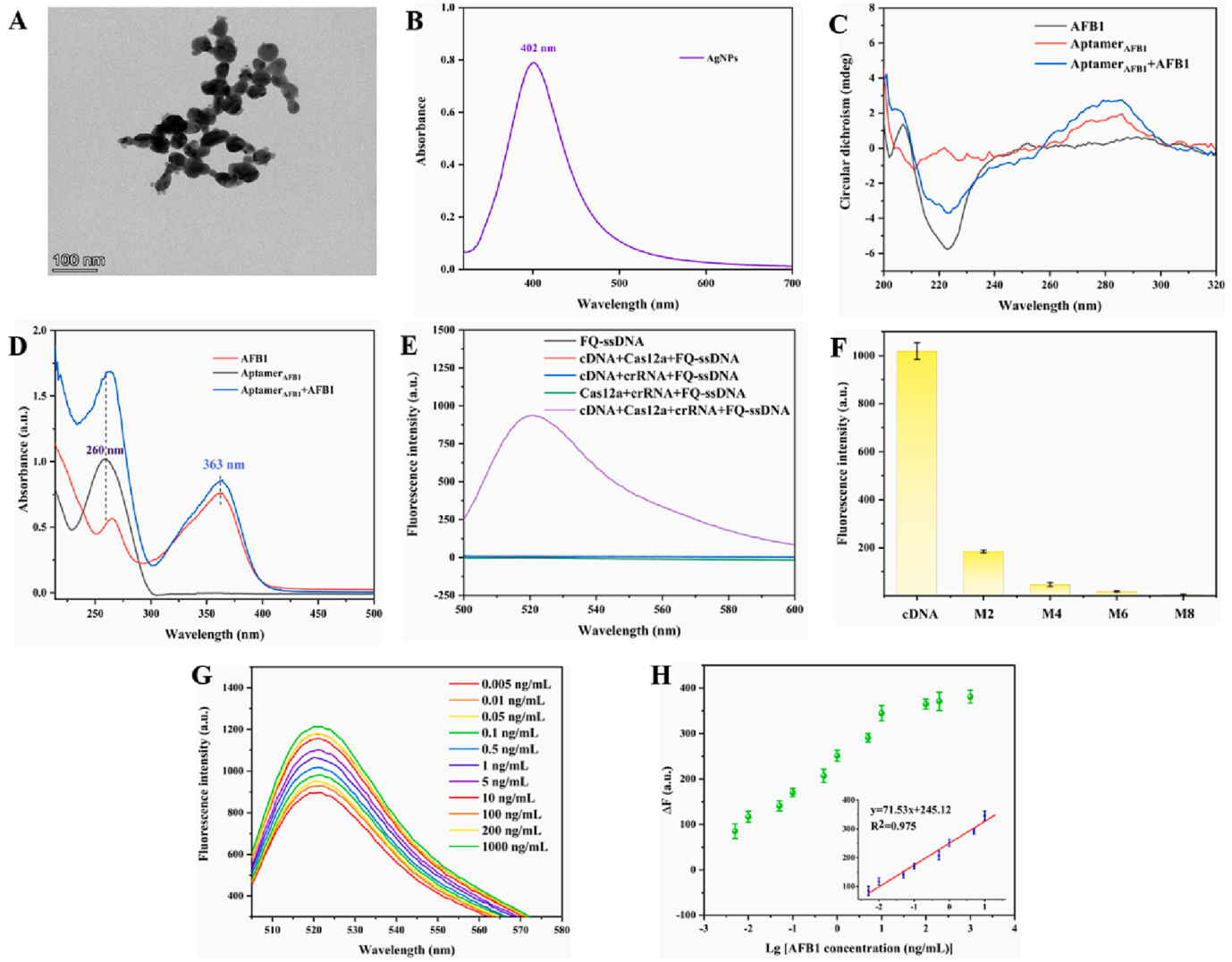


Fig. 1. TEM and UV–vis spectra of AgNPs (A and B); CD spectra (C) and UV–vis spectra (D) of AFB1, aptamer, and AFB1/aptamer complex; fluorescence feasibility verification of the FQ-ssDNA based biosensor (E); fluorescence intensity of activated Cas12a by cDNAs with different base number mismatches (F); fluorescent spectra against different concentrations AFB1 (G); the linear relationship between the fluorescent intensities and logarithmic concentration of AFB1 (H).

3.3. Feasibility of FQ reporter-based fluorescent biosensor

Target identification, *trans*-cleavage behaviour of Cas12a, and signal output were three key elements of this biosensor. The feasibility of the fluorescent biosensor was initially explored using cDNA as the activator and the conventional FQ-ssDNA reporter as cleavage substrate (Scheme 1), and the base sequence of cDNA can be paired with both aptamer and crRNA.

The recognition process of AFB1 with the specific aptamer was first verified by CD spectroscopy and UV–vis spectroscopy. The CD spectra of the aptamer (the red curve in Fig. 1C) had a negative response at 240 nm and a positive response at 280 nm, which were attributed to the helicity of the polynucleotide and the base pair stacking, respectively [44]. As shown in Fig. 1C, the CD spectra of the AFB1/aptamer complex increased at 280 nm and decreased at 240 nm due to the specific binding of AFB1 to the aptamer altering the base pair stacking and helicity of the aptamer [45]. Meanwhile, the UV–vis spectra in Fig. 1D show a classic DNA absorption peak at 260 nm for the aptamer [5]. The UV–vis absorption peak of the AFB1/Aptamer complex had the characteristic peaks of both AFB1 and the aptamer, which further demonstrated the formation of the aptamer/AFB1 complex.

To verify the *trans*-cleavage performance of Cas12a, as can be seen from Fig. 1E, significant fluorescence intensity was observed only in the presence of cDNA, Cas12a/crRNA, and FQ-ssDNA reporter simultaneously, which was due to the complementary pairing of cDNA and crRNA activating the activity of Cas12a to cleave FQ-ssDNA reporter. Notably, cDNAs with different base number mismatches could barely activate Cas12a activity (Fig. 1F). When different concentration ranges of AFB1 were added to the system, a linear increase in fluorescence signal also was observed in Fig. 1G-1H, which was attributed to the preferential formed of the aptamer/AFB1 complex, leading to the release of cDNA, while free cDNA activated the cleavage of FQ-ssDNA reporter by Cas12a.

3.4. Feasibility of G4-DNAzyme-based the multimodal biosensor

Conventional fluorescent sensing mode based on FQ-ssDNA reporter greatly increased the cost of the assay, and the use of G4-DNAzyme reporter is a promising alternative. Therefore, the feasibility of the colour development system and cleavage system of the G4-DNAzyme integrated Cas12a biosensor was explored (Fig. 2A).

3.4.1. Influence parameters of the colourimetric system

The choice of a buffer that makes the CRISPR/Cas12a cleavage

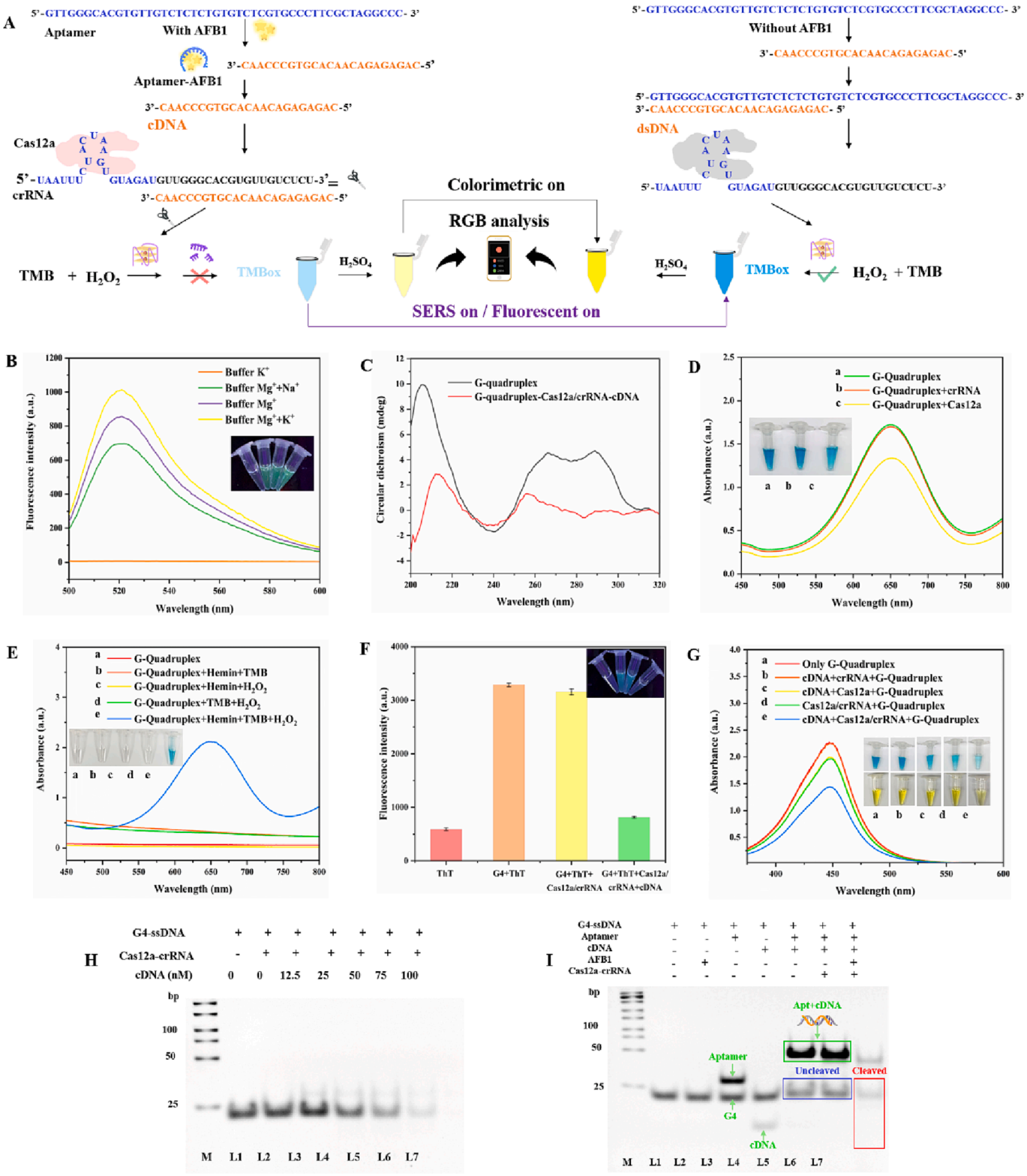


Fig. 2. Working principle of cDNA-triggered multimodal signal output (A); effect of different buffers on the *trans*-cleavage of FQ-ssDNA by Cas12a (B); CD spectra of G4 and cleaved G4 by Cas12a (C); compatibility study of G4-DNAzyme catalytic colour development system with CRISPR/Cas12a cleavage system (D); UV–vis absorption curves of intact G4-catalyzed TMB-H_2O_2 colour development reaction (E); fluorescence intensities of ThT in the presence of intact and cleaved G4 (F); verification of fluorescence feasibility based on G4 biosensor (G); fragmentation traces of activated Cas12a *trans*-cleavage G4-ssDNA at different concentrations of cDNA (H); PAGE verification of aptamer-cDNA base complementary pairing and the *trans*-cleavage activity of Cas12a protein (I).

system compatible with the G4-DNAzyme colour development system is critically important, therefore, the compatibility of different buffers was evaluated. The fluorescence experiment of Fig. 2B demonstrated that Cas12a was not activated in buffer K^+, was activated in buffer (Mg^{2+} + K^+), buffer Mg^{2+} and buffer (Mg^{2+} + Na^+), and the maximum fluorescence intensity was observed in buffer (Mg^{2+} + K^+) solution, indicating that Mg^{2+} is essential in the cleavage system [26]. Generally, the secondary structure of G4-ssDNA is mainly formed in the presence of K^+ or Na^+. To explore whether G4 could be formed successfully in the buffers of the cleavage system, CD spectra were used for characterization. The characteristic peak at 260 nm in the black curve in Fig. 2C proved the successful formation of the secondary structure of G4 in buffer (Mg^{2+} + K^+), and the position of the peak was consistent with that described in the literature [46]. To achieve successful colour development, buffer (Mg^{2+} + K^+) was ultimately chosen.

To investigate whether certain components of the cleavage system inhibited colour development, Cas12a, cDNA, and crRNA were added to the G4-DNAzyme-catalyzed colour development system, respectively. Based on the colour development results of Fig. 2D, neither cDNA nor crRNA inhibited the chromogenic system, while Cas12a slightly inhibited the chromogenic process due to a reducing agent dithiothreitol (DTT) that protects Cas12a activity [26]. Although the catalytic activity was slightly inhibited, the colour formed was sufficient for naked-eye observation.

To verify that the formed G4-DNAzyme has peroxidase-like activity, a colour development assay was conducted. As shown in Fig. 2E, only in the presence of both TMB and H_2O_2, and the DNAzyme with peroxidase-like activity formed by G4 and hemin could catalyze the oxidation of TMB [47].

3.4.2. Feasibility of the cleavage of the G4 system

Firstly, the G4 formed from G-rich ssDNA in buffer (Mg^{2+} + K^+) solution was characterized by CD spectroscopy. The black curve in Fig. 2C shows a positive response near 265 nm and a negative peak near 240 nm in the CD spectra of G4, proving the formation of the G4 hybrid structure [46]. In the presence of cDNA, the CD characteristic peak of the red curve Fig. 2C decreased dramatically, indicating that the secondary structure of G4 was disrupted. Secondly, the formation and degradation of the secondary structure of G4 can be indirectly confirmed by the principle that G4 can enhance the fluorescence intensity of thioflavin T (ThT) [48]. As shown in Fig. 2F, the fluorescence intensity of ThT itself was low, and when G4 was introduced, its fluorescence intensity was greatly enhanced, indicating the formation of a complete G4 structure. In contrast, when both Cas12a/crRNA and cDNA were present, a sharp decrease in fluorescence intensity was observed due to the cleavage of G4 by activated Cas12a. Thirdly, according to the UV–vis absorbance signal (Fig. 2G), in the presence of cDNA and Cas12a/crRNA, G4 was degraded into fragments and a decreased absorbance signal was observed at 405 nm, indicating that fragmented G4 failed to catalyze the colour development reaction. Finally, the 15% native PAGE experiment was further confirmed using 27 nt G4-ssDNA as the cleavage substrate, the results demonstrated that cDNA is essential for the activation of the Cas12a/crRNA complex, and more ssDNA was cleaved into fragments as the concentration of cDNA increased (Fig. 2H). Meanwhile, as shown in Fig. 2I, in the absence of both cDNA and Cas12a/crRNA, no traces of fragmentation of G4 were observed (lanes 1–5). In contrast, when both cDNA and aptamer were present and AFB1 was absent, cDNA preferentially bound to the aptamer to form dsDNA, thus preventing the cDNA from activating Cas12a/crRNA to cleave the G4 (lane 6). However, clear cleavage traces (lane 7) of G4 were found when AFB1 was introduced, suggesting that competitive binding of AFB1 to the aptamer resulted in free cDNA triggering the cleavage of G4-ssDNA, which was in agreement with the results of PAGE in Fig. 2H. Overall, all characterization results proved the feasibility of the CRISPR/Cas12a biosensor based on G4-DNAzyme for AFB1 detection.

3.5. Optimization of experimental conditions

To maximize the reliability of the FQ-ssDNA reporter-based sensor, vital parameters such as the concentration of Cas12a, crRNA, and FQ reporter, and the concentration ratio of the aptamer to cDNA was optimized. Firstly, different concentrations of Cas12a, crRNA and FQ reporter were chosen for fluorescence experiments, respectively. As shown in Fig. 3A-3C, from the average fluorescence intensities, the strongest fluorescence signal was achieved when the final concentrations of the three parameters were 60 nM, 90 nM, and 120 nM. To reduce the background signal, the aptamer can completely hybridize with cDNA to form dsDNA, the concentration ratio of the aptamer to cDNA was optimized, as displayed in Fig. 3D, strongest fluorescence intensity was observed when the ratio of the aptamer to cDNA was 13 nM to 15 nM. Thus, the final concentration ratio was 13 nM to 15 nM.

The optimized parameters of the cleavage system in the G4-DNAzyme-based sensor refer to the results optimized in the above fluorescence experiments. In addition, to achieve good colour development, the reaction concentration of hemin, TMB, H_2O_2, and G4-ssDNA were optimized. As shown in Fig. 3E, the UV–vis absorbance of the yellow TMBox solution at 405 nm gradually increased with increasing hemin concentration until it exceeded 2.5 μM, which was selected as the optimal concentration. Likewise, based on the UV–vis absorbance intensities, the preferred concentrations of the TMB and H_2O_2 for colourimetric signals were 0.5 mM and 4 mM (Fig. 3F and 3G), respectively. Furthermore, the concentration of G4-ssDNA was further optimized. The UV–vis absorbance intensities of the signal and background continued to increase as the concentration of G4-ssDNA increased (Fig. 3H). The signal-to-background ratio reached a maximum when the G4-ssDNA concentration was 200 nM. As such, 200 nM was considered to be the optimized concentration of G4-ssDNA.

3.6. Stability of SERS substrate and the multimodal biosensor

The assessment of the reproducibility of AgNPs substrates is crucial, 20 parallel SERS spectra (Fig. 3I) based on AgNPs substrates were measured and the calculated RSD value was 7.52%, which confirmed the excellent reproducibility of the SERS substrate (Fig. 3J). In addition, to assess the stability of the SERS substrate, AgNPs were used to detect the Raman intensity of the sensor at the same concentration of AFB1 for one week. The results in Fig. 3K showed that the SERS signals were essentially stable over seven days.

Meanwhile, the stability of the G4-DNAzyme-integrated Cas12a biosensor was also studied. Seven prepared AFB1 competitive reaction solutions were preserved at 4 °C and the UV–vis absorption signals at the same concentration of AFB1 were recorded for 7 consecutive days. As plotted in Fig. 3L, the decreasing trend of UV–vis absorbance intensity at 405 nm was not obvious, suggesting that the biosensor was relatively stable.

3.7. Sensitivity and specificity analysis of the multimodal biosensor

The quantitative applicability of the colourimetric signal was first evaluated. As shown in Fig. 4A, the UV–vis absorbance intensity at 405 nm decreased linearly with increasing AFB1 concentrations (0.001∼0.1 $ng{\cdot}mL^{-1}$), and the fitted linear equation was $y = 0.06693x + 0.2912$ ($y = F_0 - F$, x = Lg (AFB1 concentration)), corresponding coefficient of determination (R^2) of 0.977 (Fig. 4B) and a calculated LOD of 0.85 $pg{\cdot}mL^{-1}$. The colourimetric mode biosensor was integrated with the colour-assist App in the smartphone to convert colourimetric signal directly to an RGB value, further enhancing the portability for practical use. As illustrated in Fig. 4C, the calibration showed excellent linearity between the B values identified by App and logarithmic concentrations of AFB1 (0.001 to 0.1 $ng{\cdot}mL^{-1}$), and the colourimetric assay had a LOD of 1.2 pg/mL. Collectively, the biosensor simultaneously achieved semi-quantitative detection by the naked eye and quantitative determination

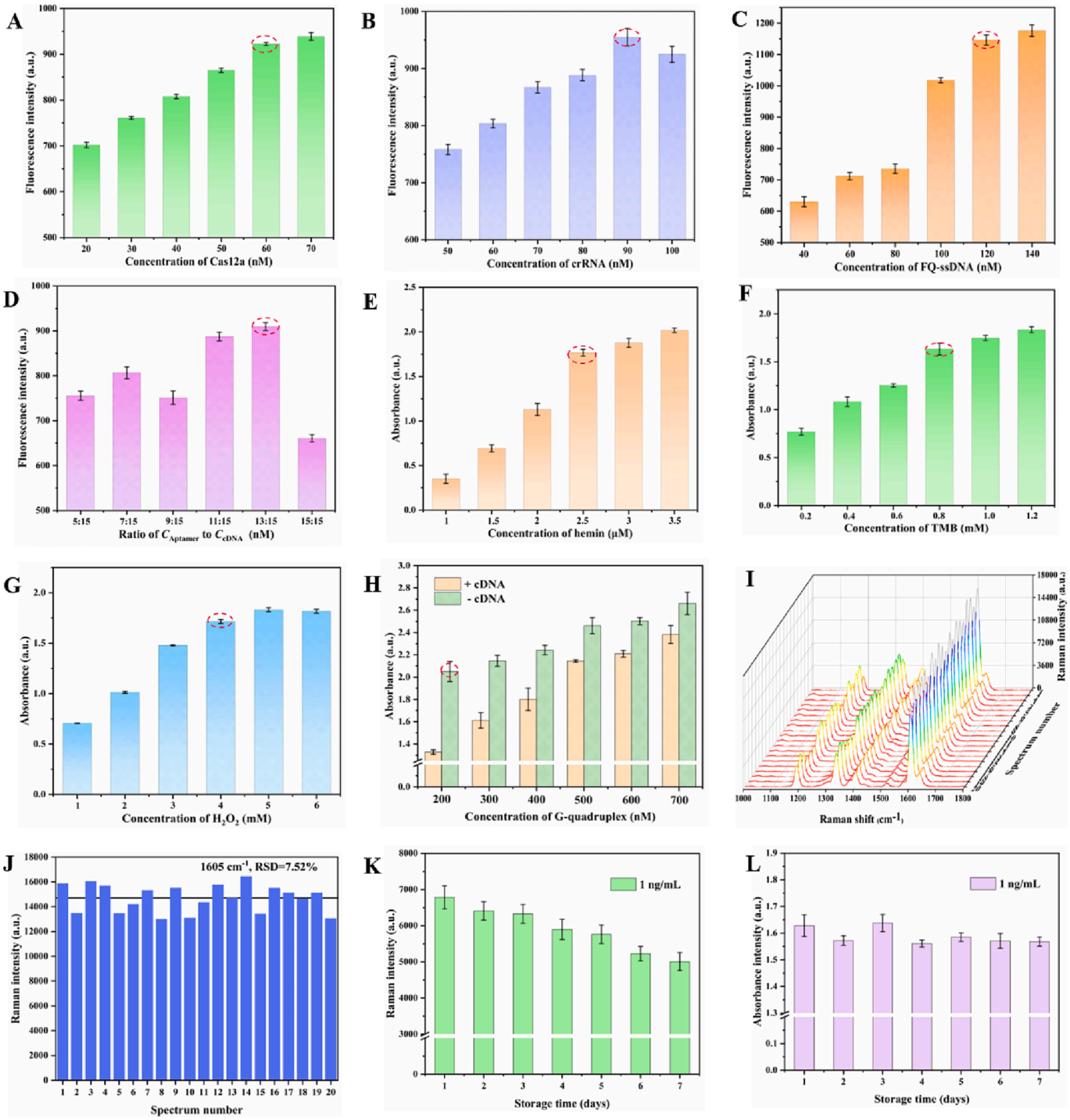


Fig. 3. Effects of different concentrations of Cas12a (cDNA: 80 nM, crRNA: 80 nM, FQ-ssDNA: 100 nM), crRNA (cDNA: 80 nM, Cas12a: 60 nM, FQ-ssDNA: 100 nM), FQ-ssDNA (cDNA: 100 nM, Cas12a: 60 nM, crRNA: 90 nM) (A, B, and C); the concentration ratio of $C_{aptamer}$ to C_{cDNA} (AFB1: 50 ng·mL^{-1}, cDNA: 90 nM, Cas12a: 60 nM, crRNA: 90 nM, FQ-ssDNA: 100 nM) (D) on fluorescence intensities; effects of different concentrations of hemin (cDNA: 50 nM, Cas12a: 60 nM, crRNA: 90 nM, G4-ssDNA: 120 nM, TMB: 600 μM, H_2O_2: 3 mM), TMB (cDNA: 50 nM, Cas12a: 60 nM, crRNA: 90 nM, G4-ssDNA: 120 nM, hemin: 2.5 μM, H_2O_2: 3 mM), H_2O_2 (cDNA: 50 nM, Cas12a: 60 nM, crRNA: 90 nM, G4-ssDNA: 120 nM, hemin: 2.5 μM, TMB: 600 μM), and G4-ssDNA (cDNA: 50 nM, Cas12a: 60 nM, crRNA: 90 nM, hemin: 2.5 μM, TMB: 600 Mm, H_2O_2: 3 mM) (E-H) on UV–vis absorbance intensities; reproducibility of the synthesized AgNPs substrate (I and J); stability of the synthesized AgNPs substrate and the developed colourimetric mode biosensor within 7 days (K and L).

by the smartphone platform, which exhibited greater advantages and potential in contamination detection. Compared to previous AFB1 detection methods (Table 1) [51,52], the assay not only had the benefits of high sensitivity and specificity but also broadened the application scope by converting target recognition into visual signal output.

The sensitivity applications of the SERS/fluorescent modes were then studied. the SERS intensity at 1605 cm^{-1} of the blue TMBox solution based on AgNPs substrate and the fluorescence intensity at 405 nm of blue TMBox solution gradually decreased with increasing AFB1 concentration (Fig. 4D and 4F). From the SERS and fluorescence standard curves in Fig. 4E and 4G, the regression equation was y = 2046.05x + 6518.17 (R^2 = 0.993) and y = 28.886x + 89.995 (R^2 =

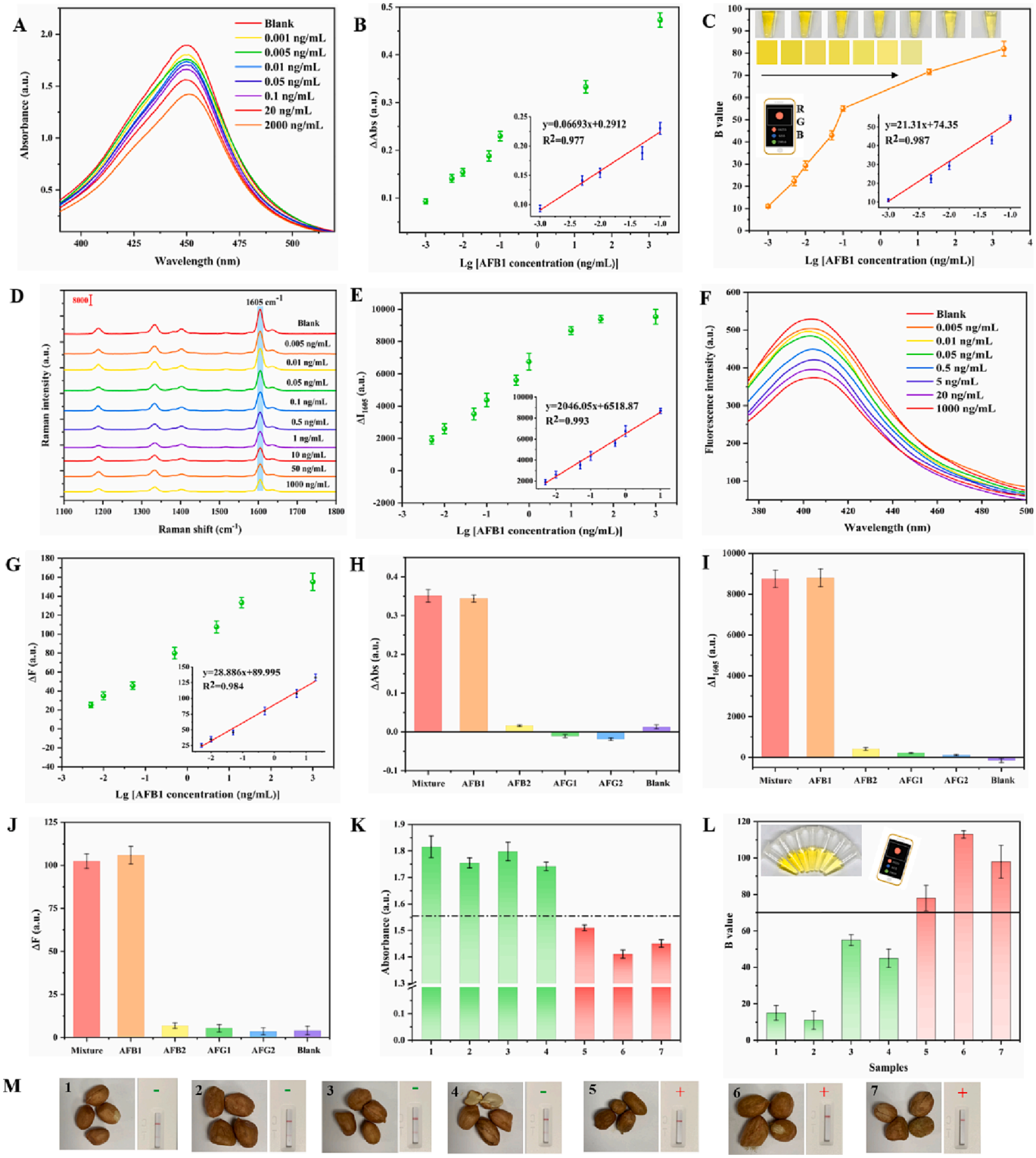


Fig. 4. UV–vis absorbance spectra against different concentrations of AFB1 (A); the linear relationship between the UV–vis intensity and logarithmic concentration of AFB1 (B); the relationship between B values identified by App in smartphone and logarithmic concentration of AFB1 based on colourimetric mode biosensor (C); SERS spectra against different concentrations of AFB1 (D); the linear relationship between the SERS intensity and logarithmic concentration of AFB1 (E); fluorescent spectra against different concentrations of AFB1 (F); the linear relationship between the fluorescent intensity and logarithmic concentration of AFB1 (G); selectivity of biosensor for different interferents (AFB1: 1 ng·mL^{-1}, AFB2/AFG1/AFG2: 10 ng·mL^{-1}) (H, I and J), quantitative determination of AFB1 in real peanut samples using UV–vis spectroscopy (K); validation of screened negative and positive samples by B-values recognized by the App in the smartphone (L); pictures of 4 positive and 3 negative real peanut samples, as well as the results of rapid screening of 7 peanut samples based on colloidal gold rapid test card (M).

Table 1
Comparison of the proposed multimodal biosensor with other biosensors for AFB1 detection.

Various biosensors	Nanomaterials	Linear range (ng·mL^{-1})	LOD (ng·mL^{-1})	Real samples	References
Electrochemistry	MoS_2/AuNPs	1.00×10^{-8}–100	0.20×10^{-7}	Rice and wheat powder	Peng et al. [4]
Electrochemistry	/	7.0×10^{-9}–5.0×10^{-7}	0.20×10^{-8}	Human serum and grape juice	Abnous et al. [53]
Colourimetry	Fe_3O_4/ Graphene oxide	10–200	/	Peanut	Hao et al. [52]
Colourimetry	Catalytic DNA circuit	0.0031–310	0.62×10^{-3}	Rice	Chen et al. [1]
Colourimetry	Magnetic bead/DNAzyme	5–100	22.6	Sorghum	Setlem et al. [54]
SERS	Fe_3O_4/Au@Ag nanorods	0.01–100	0.36×10^{-2}	Peanut oil	Chen et al. [51]
SERS	Fe_3O_4@Au nanoflowers	0.0001–100	0.40×10^{-3}	Peanut oil	He et al. [55]
SERS	Au NP dimers/MXenes	0.001–100	0.60×10^{-3}	Peanut	Wu et al. [5]
Fluorescence	Fe_3O_4/DNAzyme	0.5–15	0.20×10^{-1}	Cereal	Wang et al. [50]
Fluorescence	QDs/AuNPs	0.05–100	0.20×10^{-1}	Peanut	Lu et al. [49]
Fluorescence	Cas12a and MXenes	0.001–80	0.92×10^{-3}	Peanut	Wu et al. [11]
Fluorescence	Fe_3O_4@MoS_2-NGQDs	0.001–10	0.31×10^{-3}	Peanut	Jia et al. [56]
FRET	MoS_2 nanosheet	0.01–10	3.30×10^{-3}	Peanut	Qian et al. [57]
Colourimetry		0.001–0.1	0.85×10^{-3}		
SERS	Cas12a and G4-DNAzyme	0.005–10	0.79×10^{-3}	Peanut, maize, and badam	This work
Fluorescence		0.005–20	0.17×10^{-2}		

Note: FRET = Fluorescence resonance energy transfer.

0.984), respectively, and X and Y represent the same meaning as colourimetric mode. Remarkably, LODs as low as 0.79 pg·mL^{-1} and 1.65 pg·mL^{-1} for SERS and fluorescence modes, respectively, indicating the potential application of the current detection platform in the detection of AFB1 by comparing it with references as listed in Table 1.

The anti-interference ability of the multimodal biosensor was verified by detecting a blank control, three interferers, AFB2, AFG1, and AFG1, which readily coexist in AFB1, and a mixture of the three toxins. As shown in Fig. 4H, 4I, and 4 J, the signals of the experimental groups in the presence of AFB1 were all significantly enhanced, while the three interferer groups and the blank group showed almost no change, which was attributed to the release of cDNA due to the presence of AFB1. Thus, the proposed multimodal sensing platform exhibited promising specificity.

3.8. Application in spiked and real samples detection

Spiked recovery experiments based on the proposed sensor for the detection of AFB1 in peanut, maize, and badam samples at concentrations of 10, 1.0, and 0.1 ng·mL^{-1}, respectively. Satisfactory recoveries were achieved for all three different types of food-spiked samples in colourimetric, SERS, and fluorescence modes (Table 2). Meanwhile, the spiked samples were also assayed by a classical ELISA approach, and the results in Table 2 showed that the multimodal sensor has a promising application in detecting spiked samples.

To prove the future application of the proposed approach in real samples, 7 samples of peanuts naturally contaminated with AFB1 were first measured with the colloidal gold-based AFB1 test card, of which 4 were positive and 3 were negative (Fig. 4M). Subsequently, 7 samples were assessed based on the designed biosensor, and the UV–vis absorbance results in Fig. 4K indicated that the sensor was practicable in real sample applications. More importantly, the results of B values in Fig. 4L show that the proposed colourimetric mode sensor correctly recognized both positive and negative samples, thereby endorsing the potential application of this smartphone-assisted biosensor in real samples.

As shown in Table 1, currently, most biosensors [4,49,51,52] for AFB1 detection required the synthesis and self-assembly of various materials, which increased the complexity of experiments and limited the rapid detection of AFB1 in practical applications. The designed CRISPR/cas12a biosensor was the advantage of simple operation, and rapid, sensitive, and specific detection. Also, CRISPR/cas12a biosensors were mostly fluorescence-based signals, which always rely on expensive chemically-modified FQ-ssDNA probes. Compared with existing methods, the cheap G4-DNAzyme was integrated into the CRISPR/Cas12a detection system and was used to catalyze the colour development reaction of TMB-H_2O_2. This strategy achieved a simultaneous output of colourimetric, SERS, and fluorescence signals, and the final solution colour could be directly observed by the naked eye, as well as indirectly identified using the colour-assist App on a smartphone. More importantly, the superior cleavage behaviour of CRISPR/Cas12a simultaneously realized signal conversion of small molecule, Cas12a-driven, and amplified output signals, significantly improving the stability, specificity, and sensitivity of the analytical method.

4. Conclusions

In summary, a novel multimodal sensor platform was proposed based on the CRISPR/Cas12a coupled with G4-DNAzyme for the detection of AFB1. Meanwhile, a conventional fluorescent biosensor with an FQ-ssDNA reporter as the cleavage substrate was used as a comparison strategy. In short, AFB1 triggered the cleavage of G4 by Cas12a, resulting in the deprivation of peroxidase-like activity of G4-DNAzyme,

Table 2
Detection of AFB1 in spiked peanut, maize, and badam samples based on the multimodal biosensor and ELISA method.

Samples	Spiked (ng·mL^{-1})	Colourimetric		SERS		Fluorescent		ELISA	
		Detected (ng·mL^{-1}, mean ± SD)	Recovery (%)	Detected (ng·mL^{-1}, mean ± SD)	Recovery (%)	Detected (ng·mL^{-1}, mean ± SD)	Recovery (%)	Detected (ng·mL^{-1}, mean ± SD)	Recovery (%)
Peanut	10.0	9.512 ± 0.29	95.1	8.912 ± 0.539	89.1	9.179 ± 0.194	91.8	10.128 ± 0.521	101.3
	1.00	0.831 ± 0.051	83.1	0.963 ± 0.061	96.3	0.902 ± 0.037	90.2	0.898 ± 0.062	89.8
	0.10	0.093 ± 0.002	93.0	0.088 ± 0.004	88.0	0.084 ± 0.001	84.0	0.0925 ± 0.005	92.5
Maize	10.0	8.792 ± 0.19	87.9	9.237 ± 0.314	92.4	10.852 ± 0.324	108.5	8.566 ± 0.27	85.7
	1.00	1.083 ± 0.031	108.3	0.896 ± 0.029	89.6	0.895 ± 0.053	89.5	0.971 ± 0.042	97.1
	0.10	0.086 ± 0.015	86.0	0.091 ± 0.006	91.0	0.094 ± 0.004	94.0	0.088 ± 0.007	88.0
Badam	10.0	10.197 ± 0.33	102.0	10.68 ± 0.11	106.8	8.992 ± 0.37	89.9	9.178 ± 0.39	91.8
	1.00	0.969 ± 0.07	96.9	0.859 ± 0.048	85.9	0.926 ± 0.024	92.6	0.881 ± 0.038	88.1
	0.10	0.084 ± 0.004	84.0	0. 091 ± 0.001	91.0	0. 086 ± 0.003	86.0	0.090 ± 0.007	90.0

therefore, the UV–vis absorbance, fluorescence, and SERS intensities of the sensing platform were significantly changed, and the colourimetric signals could be integrated into the colour-assist App in the smartphone. The multi-signal output sensor exhibited a wide detection range and low detection limits. Furthermore, the biosensor was also applicable to the evaluation of spiking experiments in real peanut, maize, and badam samples, further demonstrating the practicability of the sensor in AFB1 detection. Remarkably, the proposed smartphone-assisted colourimetric mode sensor realized correct recognition between positive and negative samples in 7 peanut samples, confirming the practicability in the real samples. To sum up, the specific binding between AFB1 and the aptamer ensured the effective identification of the target, the *trans*-cleavage activity of Cas12a amplified the output signals, and the G4-DNAzyme reporter reduced the cost of detection and achieved a simultaneous output of all three signals compared to the FQ reporter. More importantly, the multimodal biosensor provided new insights and bring innovative inspiration to exploring the detection of various analytes.

CRediT authorship contribution statement

Zhihui Wu: Writing – original draft, Formal analysis, Investigation. **Da-Wen Sun:** Supervision, Funding acquisition, Resources, Writing – review & editing. **Hongbin Pu:** Validation, Funding acquisition, Resources.

Declaration of Competing Interest

The authors declare that they have no known competing financial interests or personal relationships that could have appeared to influence the work reported in this paper.

Data availability

The authors are unable or have chosen not to specify which data has been used.

Acknowledgements

The authors are grateful to the Guangzhou Key Laboratory for Intelligent Sensing and Quality Control of Agricultural Products (202102100009) for its support. This research was also supported by the Common Technical Innovation Team of Guangdong Province on Preservation and Logistics of Agricultural Products (2023KJ145), the Guangdong Provincial Science and Technology Plan Projects (2020A1414010160), and the Guangdong Basic and Applied Basic Research Foundation (2022A1515012489).

References

[1] J. Chen, J. Wen, L. Zhuang, S. Zhou, An enzyme-free catalytic DNA circuit for amplified detection of aflatoxin B1 using gold nanoparticles as colourimetric indicators, Nanoscale 8 (18) (2016) 9791–9797.
[2] H. He, D.-W. Sun, H. Pu, Z. Wu, A SERS-fluorescence dual-signal aptasensor for sensitive and robust determination of AFB1 in nut samples based on Apt-Cy5 and MNP@Ag-PEI, Talanta 253 (2022), 123962.
[3] Z. Wu, D.-W. Sun, H. Pu, Q. Wei, A dual signal-on biosensor based on dual-gated locked mesoporous silica nanoparticles for the detection of Aflatoxin B1, Talanta 253 (2022), 124027.
[4] G. Peng, X. Li, F. Cui, Q. Qiu, X. Chen, H. Huang, Aflatoxin B1 electrochemical aptasensor based on tetrahedral DNA nanostructures functionalized three dimensionally ordered macroporous MoS_2-AuNPs film, ACS Appl. Mater. Interf. 10 (21) (2018) 17551–17559.
[5] Z. Wu, D.-W. Sun, H. Pu, Q. Wei, X. Lin, Ti_3C_2Tx MXenes loaded with Au nanoparticle dimers as a surface-enhanced Raman scattering aptasensor for AFB1 detection, Food Chem. 372 (2022), 131293.
[6] H. Jayan, D.-W. Sun, H. Pu, Q. Wei, Mesoporous silica coated core-shell nanoparticles substrate for size-selective SERS detection of chloramphenicol, Spectrochim. Acta A Mol. Biomol. Spectrosc. 284 (2023), 121817.
[7] L. Huang, D.-W. Sun, Z. Wu, H. Pu, Q. Wei, Reproducible, shelf-stable, and bioaffinity SERS nanotags inspired by multivariate polyphenolic chemistry for bacterial identification, Anal. Chim. Acta 1167 (2021), 338570.
[8] B. Zetsche, J. Gootenberg, O. Abudayyeh, I. Slaymaker, K. Makarova, P. Essletzbichler, S. Volz, J. Joung, J. van der Oost, A. Regev, E. Koonin, F. Zhang, Cpf1 is a single RNA-guided endonuclease of a class 2 CRISPR-Cas system, Cell 163 (3) (2015) 759–771.
[9] S. Konermann, M. Brigham, A. Trevino, J. Joung, O. Abudayyeh, C. Barcena, P. Hsu, N. Habib, J. Gootenberg, H. Nishimasu, O. Nureki, F. Zhang, Genome-scale transcriptional activation by an engineered CRISPR-Cas9 complex, Nature 517 (7536) (2015) 583–588.
[10] H. Rahimi, M. Salehiabar, M. Barsbay, M. Ghaffarlou, T. Kavetskyy, A. Sharafi, S. Davaran, S. Chauhan, H. Danafar, S. Kaboli, H. Nosrati, M. Yallapu, J. Conde, CRISPR systems for COVID-19 diagnosis, ACS Sensors 6 (4) (2021) 1430–1445.
[11] Z. Wu, D.-W. Sun, H. Pu, Q. Wei, A novel fluorescence biosensor based on CRISPR/Cas12a integrated MXenes for detecting aflatoxin B1, Talanta 252 (2022), 123773.
[12] J. Chen, E. Ma, L. Harrington, M. Costa, X. Tian, J. Palefsky, J. Doudna, CRISPR-Cas12a target binding unleashes indiscriminate single-stranded DNase activity, Science 360 (2018) 436–439.
[13] Y. Dai, R. Somoza, L. Wang, J. Welter, Y. Li, A. Caplan, C. Liu, Exploring the trans-cleavage activity of CRISPR-Cas12a (cpf1) for the development of a universal electrochemical biosensor, Angew. Chem. Int. Ed. 58 (48) (2019) 17399–17405.
[14] H. Gong, Y. Wu, R. Zeng, Y. Zeng, X. Liu, D. Tang, CRISPR/Cas12a-mediated liposome-amplified strategy for the photoelectrochemical detection of nucleic acid, Chem. Commun. (Camb) 57 (71) (2021) 8977–8980.
[15] Y. Chen, N. Zong, F. Ye, Y. Mei, J. Qu, X. Jiang, Dual-CRISPR/Cas12a-assisted RT-RAA for ultrasensitive SARS-CoV-2 detection on automated centrifugal microfluidics, Anal. Chem. 94 (27) (2022) 9603–9609.
[16] F. Deng, Y. Li, B. Li, E.M. Goldys, Increasing trans-cleavage catalytic efficiency of Cas12a and Cas13a with chemical enhancers: application to amplified nucleic acid detection, Chem. Sensors Actuators B 373 (2022), 132767.
[17] C. Wang, J. Qian, K. Wang, M. Hua, Q. Liu, N. Hao, T. You, X. Huang, Nitrogen-doped graphene quantum dots@SiO_2 nanoparticles as electrochemiluminescence and fluorescence signal indicators for magnetically-controlled aptasensor with dual detection channels, ACS Appl. Mater. Interfaces 7 (48) (2015) 26865–26873.
[18] C. Wang, X. Zhao, C. Gu, F. Xu, W. Zhang, X. Huang, J. Qian, Fabrication of a versatile aptasensing chip for aflatoxin B1 in photothermal and electrochemical dual modes, Food Anal. Methods 15 (12) (2022) 3390–3399.
[19] B. Qiao, J. Xu, W. Yin, W. Xin, L. Ma, J. Qiao, Y. Liu, "Aptamer-locker" DNA coupling with CRISPR/Cas12a-guided biosensing for high-efficiency melamine analysis, Biosens. Bioelectron. 183 (2021), 113233.
[20] X. Lin, C. Li, X. Meng, W. Yu, N. Duan, Z. Wang, S. Wu, CRISPR-Cas12a-mediated luminescence resonance energy transfer aptasensing platform for deoxynivalenol using gold nanoparticle-decorated Ti_3C_2Tx MXene as the enhanced quencher, J. Hazard. Mater. 433 (2022), 128750.
[21] J. Zhao, Z. Tan, L. Wang, C. Lei, Z. Nie, A ligation-driven CRISPR-Cas biosensing platform for non-nucleic acid target detections, Chem. Commun. (Camb) 57 (57) (2021) 7051–7054.
[22] M. Qing, S. Chen, Z. Sun, Y. Fan, H. Luo, N. Li, Universal and programmable rolling circle amplification-CRISPR/Cas12a-mediated immobilization-free electrochemical biosensor, Anal. Chem. 93 (20) (2021) 7499–7507.
[23] M. Zhang, X. Xue, H. Gong, B. Liu, L. Ye, Double isothermal amplification and CRISPR-Cas12a for sensitive detection of citrinin, ACS Food Sci. Technol. 1 (10) (2021) 1997–2005.
[24] L. Huang, D.-W. Sun, H. Pu, Photosensitized peroxidase mimicry at the hierarchical 0D/2D heterojunction-like quasi metal-organic framework interface for boosting biocatalytic disinfection, Small 18 (20) (2022) e2200178.
[25] L. Yin, N. Duan, S. Chen, Y. Yao, J. Liu, L. Ma, Ultrasensitive pathogenic bacteria detection by a smartphone-read G-quadruplex-based CRISPR-Cas12a bioassay, Sensors Actuat. B: Chem. 347 (2021), 130586.
[26] X. Chen, L. Wang, F. He, G. Chen, L. Bai, K. He, F. Zhang, X. Xu, Label-free colourimetric method for detection of vibrio parahaemolyticus by trimming the G-quadruplex DNAzyme with CRISPR/Cas12a, Anal. Chem. 93 (42) (2021) 14300–14306.
[27] D. Li, Z. Zhu, D.-W. Sun, Visualization and quantification of content and hydrogen bonding state of water in apple and potato cells by confocal Raman microscopy: a comparison study, Food Chem. 385 (2022), 132679.
[28] H. Shen, A. Qileng, H. Yang, H. Liang, H. Zhu, Y. Liu, H. Lei, W. Liu, "Dual-signal-On" integrated-type biosensor for portable detection of miRNA: Cas12a-induced photoelectrochemistry and fluorescence strategy, Anal. Chem. 93 (34) (2021) 11816–11825.
[29] R. Pan, J. Liu, P. Wang, D. Wu, J. Chen, Y. Wu, G. Li, Ultrasensitive CRISPR/Cas12a-Driven SERS biosensor for on-site nucleic acid detection and its application to milk authenticity testing, J. Agric. Food Chem. 70 (14) (2022) 4484–4491.
[30] H. Pu, H. Zhu, F. Xu, D.-W. Sun, Development of core-satellite-shell structured MNP@Au@MIL-100(Fe) substrates for surface-enhanced Raman spectroscopy and their applications in trace level determination of malachite green in prawn, J. Raman Spectrosc. 53 (4) (2022) 682–693.
[31] H. Jayan, D.-W. Sun, H. Pu, Q. Wei, Surface-enhanced Raman spectroscopy combined with stable isotope probing to assess the metabolic activity of Escherichia coli cells in chicken carcass wash water, Spectrochim. Acta A Mol. Biomol. Spectrosc. 280 (2022), 121549.
[32] D. Li, Z. Zhu, D.-W. Sun, Quantification of hydrogen bonding strength of water in saccharide aqueous solutions by confocal Raman microscopy, J. Mol. Liq. 342 (2021), 117498.
[33] H. He, D.-W. Sun, Z. Wu, H. Pu, Q. Wei, On-off-on fluorescent nanosensing: materials, detection strategies and recent food applications, Trends Food Sci. Technol. 119 (2022) 243–256.

[34] O. Mukama, J. Wu, Z. Li, Q. Liang, Z. Yi, X. Lu, Y. Liu, Y. Liu, M. Hussain, G. Makafe, J. Liu, N. Xu, L. Zeng, An ultrasensitive and specific point-of-care CRISPR/Cas12 based lateral flow biosensor for the rapid detection of nucleic acids, Biosens. Bioelectron. 159 (2020), 112143.
[35] D. Li, C. Li, A. Liang, Z. Jiang, SERS and fluorescence dual-mode sensing trace hemin and K^+ based on G-quarplex/hemin DNAzyme catalytic amplification, Chem. Sensors Actuators B 297 (2019), 126799.
[36] J. Qian, C. Ren, C. Wang, K. An, H. Cui, N. Hao, K. Wang, Gold nanoparticles mediated designing of versatile aptasensor for colorimetric/electrochemical dual-channel detection of aflatoxin B1, Biosens. Bioelectron. 166 (2020), 112443.
[37] L. Chen, X. Fu, J. Li, Ultrasensitive surface-enhanced Raman scattering detection of trypsin based on anti-aggregation of 4-mercaptopyridine-functionalized silver nanoparticles: an optical sensing platform toward proteases, Nanoscale 5 (13) (2013) 5905–5911.
[38] C. Zhang, L. Huang, H. Pu, D.-W. Sun, Magnetic surface-enhanced Raman scattering (MagSERS) biosensors for microbial food safety: Fundamentals and applications, Trends Food Sci. Technol. 113 (2021) 366–381.
[39] D. Zhang, H. Pu, L. Huang, D.-W. Sun, Advances in flexible surface-enhanced Raman scattering (SERS) substrates for nondestructive food detection: fundamentals and recent applications, Trends Food Sci. Technol. 109 (2021) 690–701.
[40] Y. Xiong, J. Zhang, Z. Yang, Q. Mou, Y. Ma, Y. Xiong, Y. Lu, Functional DNA regulated CRISPR-Cas12a sensors for point-of-care diagnostics of non-nucleic-acid targets, J. Am. Chem. Soc. 142 (1) (2020) 207–213.
[41] T. Li, R. Hu, J. Xia, Z. Xu, D. Chen, J. Xi, B. Liu, J. Zhu, Y. Li, Y. Yang, M. Liu, G-triplex: A new type of CRISPR-Cas12a reporter enabling highly sensitive nucleic acid detection, Biosens. Bioelectron. 187 (2021), 113292.
[42] Y. Yu, S. Xue, C. Zhao, B. Barnych, G. Sun, Highly sensitive, selective, and reusable nanofibrous membrane-based carbon polymer dots sensors for detection of Cr (VI) in water, Appl. Surf. Sci. 582 (2022), 152392.
[43] J. Hu, H. Song, J. Zhou, R. Liu, Y. Lv, Metal-tagged CRISPR/Cas12a bioassay enables ultrasensitive and highly selective evaluation of kanamycin bioaccumulation in fish samples, Anal. Chem. 93 (42) (2021) 14214–14222.
[44] N. Garbett, P. Ragazzon, J. Chaires, Circular dichroism to determine binding mode and affinity of ligand-DNA interactions, Nat. Protoc. 2 (12) (2007) 3166–3172.
[45] C. Wang, K. Zhu, P. Shi, X. Ding, S. Zhang, Rapid and label-free detection of aflatoxin B1 using a rationally truncated aptamer and via circular dichroism measurement, Chem. Commun. (Camb) 58 (30) (2022) 4779–4782.
[46] Y. Li, T. Li, B.F. Liu, R. Hu, J. Zhu, T. He, X. Zhou, C. Li, Y. Yang, M. Liu, CRISPR-Cas12a trans-cleaves DNA G-quadruplexes, Chem. Commun. (Camb) 56 (83) (2020) 12526–12529.
[47] Y. Huang, Y. Gu, X. Liu, T. Deng, S. Dai, J. Qu, G. Yang, L. Qu, Reusable ring-like Fe_3O_4/Au nanozymes with enhanced peroxidase-like activities for colourimetric-SERS dual-mode sensing of biomolecules in human blood, Biosens. Bioelectron. 209 (2022), 114253.
[48] S. Jing, Q. Liu, Y. Jin, B. Li, Dimeric G-quadruplex: an effective nucleic acid scaffold for lighting up thioflavin T, Anal. Chem. 93 (3) (2021) 1333–1341.
[49] X. Lu, C. Wang, J. Qian, C. Ren, K. An, K. Wang, Target-driven switch-on fluorescence aptasensor for trace aflatoxin B1 determination based on highly fluorescent ternary CdZnTe quantum dots, Anal. Chim. Acta 1047 (2019) 163–171.
[50] L. Wang, F. Zhu, M. Chen, Y. Zhu, J. Xiao, H. Yang, X. Chen, Rapid and visual detection of aflatoxin B1 in foodstuffs using aptamer/G-quadruplex DNAzyme probe with low background noise, Food Chem. 271 (2019) 581–587.
[51] Q. Chen, M. Yang, X. Yang, H. Li, Z. Guo, M. Rahma, A large Raman scattering cross-section molecular embedded SERS aptasensor for ultrasensitive aflatoxin B1 detection using CS-Fe_3O_4 for signal enrichment, Spectrochim. Acta A Mol. Biomol. Spectrosc. 189 (2018) 147–153.
[52] N. Hao, J. Lu, Z. Zhou, R. Hua, K. Wang, A pH-resolved colourimetric biosensor for simultaneous multiple target detection, ACS Sensors 3 (10) (2018) 2159–2165.
[53] K. Abnous, N.M. Danesh, M. Alibolandi, M. Ramezani, A. Sarreshtehdar Emrani, R. Zolfaghari, S.M. Taghdisi, A new amplified pi-shape electrochemical aptasensor for ultrasensitive detection of aflatoxin B1, Biosensors Bioelectron. 94 (2017) 374–379.
[54] S. Setlem, B. Mondal, S. Ramlal, A fluorescent aptasensor for the detection of aflatoxin B1 by graphene oxide mediated quenching and release of fluorescence, J. Microbiol. Methods 193 (2022), 106414.
[55] H. He, D.-W. Sun, H. Pu, L. Huang, Bridging Fe_3O_4@Au nanoflowers and Au@Ag nanospheres with aptamer for ultrasensitive SERS detection of aflatoxin B1, Food Chem. 324 (2020), 126832.
[56] S. Jia, C. Wang, J. Qian, X. Zhang, H. Cui, Q. Zhang, Y. Tian, N. Hao, J. Wei, K. Wang, An upgraded 2D nanosheet-based FRET biosensor: insights into avoiding background and eliminating effects of background fluctuations, Chem. Commun. 58 (3) (2022) 467–470.
[57] J. Qian, H. Cui, X. Lu, C. Wang, K. An, N. Hao, K. Wang, Bi-color FRET from two nano-donors to a single nano-acceptor: A universal aptasensing platform for simultaneous determination of dual targets, Chem. Eng. J. 401 (2020), 126017.